JOURNAL OF SOLID STATE CHEMISTRY 67, 297–307 (1987)

Synthesis and Characterization of a New Calcium Platinum Oxide: $Ca_2Pt_3O_8$

X. TURRILLAS,*,† C. LAVIRON,‡ H. VINCENT,‡ J. PANNETIER,§ AND J. C. JOUBERT*

Laboratoire de Matériaux et de Génie Physique, U.A. 1009 Ensieg, BP 46, F-38402 St Martin d'Hères, France; ‡Laboratoire de Cristallographie, CNRS, Laboratoire associé à l'USMG, 166 X, F-38042 Grenoble Cedex, France; and §Institut Laue—Langevin, F-38042 Grenoble Cedex, France

Received October 16, 1985; in revised form May 9, 1986

$Ca_2Pt_3O_8$ was prepared by treatment of $CaPt(OH)_6$ under hydrothermal conditions (800 K and 170 MPa for 12 hr). The structure was determined by powder X-ray and neutron diffraction. The space group is $R\bar{3}m$, and the cell parameters in the hexagonal system are a = 6.196 Å, c = 15.404 Å, with three formula units per unit cell. Thermal stability of $Ca_2Pt_3O_8$ was also studied, by means of TGA and DTA techniques.

1. Introduction

In the last few years the chemistry of platinum ternary oxides has seen considerable progress. This interest is due mainly to the potential use of their catalytic and electrochemical properties. In fact, semiconductor, insulator, and metallic-conductor ternary platinum oxides have been reported. In a recent review by Schwartz and Prewitt (*1*) the structure and properties of binary and ternary oxides known at present can be seen with some detail.

In the Ca–Pt–O system four phases were reported: $CaPt_2O_4$ (*2*) is tetragonal with cell parameters a = 5.774 Å and c = 5.588 Å; for the formula Ca_4PtO_6 there are two polymorphs, one of which is orthorhombic (*3, 4*) with cell parameters a = 9.18 Å, b = 9.24 Å, and c = 6.50 Å, and the other (*5, 6*), isostructural with Sr_4PtO_6, is trigonal with a = 9.3308(1) Å and c = 11.246(1) Å; and finally, Laviron (*7*) obtained the orthorhombic phase $CaPt_3O_6$, isostructural with $CdPt_3O_6$ (*8*), with cell dimensions a = 6.250 Å, b = 11.771 Å, and c = 3.189 Å. This paper reports the preparation and characterization of a new crystalline phase with composition $Ca_2Pt_3O_8$.

2. Experimental

2.1. Synthesis. Starting materials were of reagent grade quality. In a typical experiment 0.3 g of $CaPt(OH)_6$ was mixed with 0.6 ml of distilled water and introduced into a platinum or gold tube, which was then sealed by welding. The mixture occupied 30% of the volume of the tube. The tube

† To whom correspondence should be addressed: Wolfson Unit for Solid State Ionics, Department of Metallurgy & Materials Science, Imperial College of Science & Technology, Prince Consort Rd., London SW7 2BP, U.K.

0022-4596/87 $3.00

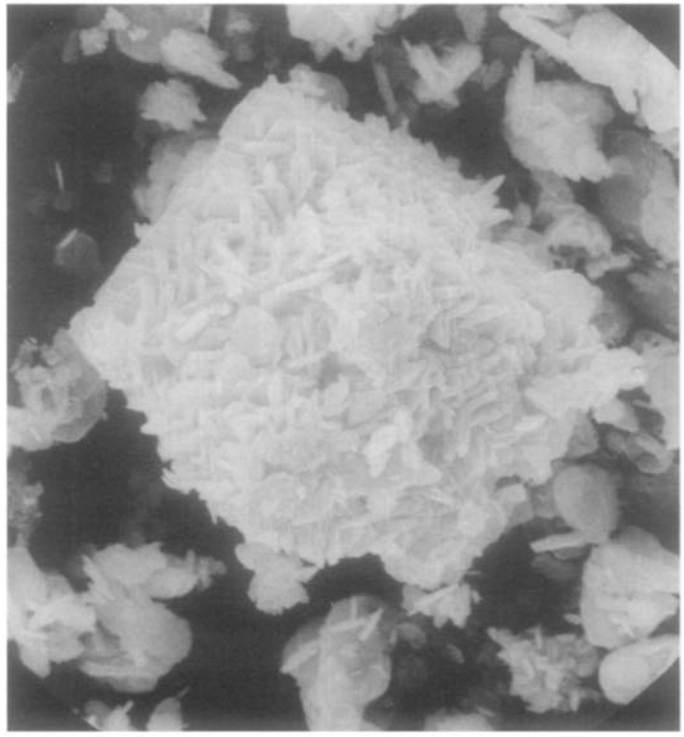

FIG. 1. SEM photograph of $Ca_2Pt_3O_8$. ×200.

was placed in an autoclave under a pressure of 170 MPa at a temperature of about 800 K for 12 hr. After that, in some cases the temperature and pressure were lowered slowly (for 4 days) and in other cases faster (12 hr). Finally, the yellow powder of $Ca_2Pt_3O_8$ was washed with hot aqua regia for 2 hr, then washed with distilled water, and dried at 150°C for 2 hr.

$CaPt(OH)_6$ was obtained as follows: 10 g of hexachloroplatinic acid, $H_2PtCl_6 \cdot H_2O$, was dissolved in 20 ml of distilled water, 12 g of KOH (84%) was dissolved in 80 ml of water, and the solutions were mixed. A yellow precipitate appeared which was dissolved by means of a magnetic stirrer and heating to 80°C. This treatment was carried out for 12 hr until a golden yellow solution of $Pt(OH)_6^{2-}$ was obtained. This solution was then diluted up to 500 ml, the pH was adjusted, and a 0.5 *M* $CaCl_2$ solution was added drop by drop with continuous stir-

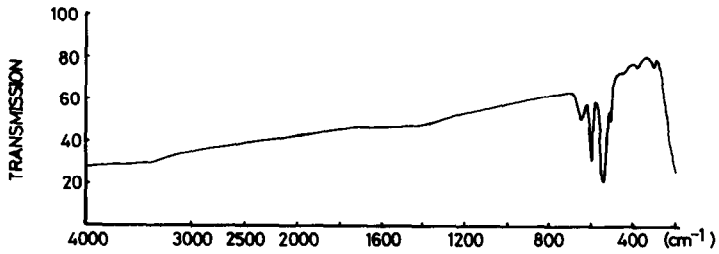

FIG. 2. Infrared spectra of $Ca_2Pt_3O_8$.

TABLE I

THERMAL DECOMPOSITION OF $Ca_2Pt_3O_8$[a]

t (°C)	Time (hr)	Phases detected
450	2	$Ca_2Pt_3O_8$
500	1	$Ca_2Pt_3O_8$
550	1	$Ca_2Pt_3O_8$
600	2	$Ca_2Pt_3O_8$ + Pt
650	1	$Ca_2Pt_3O_8$ + Pt
700	2	$Ca_2Pt_3O_8$ + Pt
750	1	$Ca_2Pt_3O_8$ + Pt
800	1	$Ca_2Pt_3O_8$ + Pt
850	2	$CaPt_2O_4$ + Ca_4PtO_6(trig) + Pt
900	1	$CaPt_2O_4$ + Ca_4PtO_6(trig) + Pt
950	1	Ca_4PtO_6(trig) + Pt
1000	1	Ca_4PtO_6(trig) + Pt
1100	1	Pt

[a] Phases detected by means of X-ray diffraction after each thermal treatment.

TABLE II

THERMAL DECOMPOSITION OF $Ca_2Pt_3O_8$[a]

Reaction	t (°C)	Weight loss (%)
(1) $Ca_2Pt_3O_8 \rightarrow$ Pt + Cao	720	1.48
(2) $Ca_2Pt_3O_8 \rightarrow CaPt_2O_4 + Ca_4PtO_6$ + Pt + CaO	855	8.69
(3) $CaPt_2O_4 \rightarrow$ Pt + CaO	960	11.49
(4) $Ca_4PtO_6 \rightarrow$ Pt + CaO	1130	12.54

[a] Weight loss and temperature for each step.

ring. Finally, the pale-yellow precipitate of $CaPt(OH)_6$ was filtered, washed with distilled water, and dried at 120°C for 12 hr.

2.2. Thermal analysis. DTA and TGA diagrams were obtained with a SETARAM thermobalance. The samples were placed in platinum boats in air and the temperature was measured with a Pt–Rh(6%)–Pt–Rh(30%) thermocouple. The heating rate was controlled by applying a linear emf of 1 mV/hr (≈100°C/hr between 800 and 1000°C).

2.3. Infrared spectrometry. The apparatus used was a Perkin–Elmer 283 double beam, and the spectrometer region scanned was 200 to 4000 cm^{-1}. The sample was mixed with dried KBr and pressed to obtain transparent pellets.

2.4. Scanning electron microscopy. The images of the samples, covered with a sputtered gold layer, were obtained using a SEM JEOL JSM 35 CF.

2.5. Measurement of density. Density was determined by weighing successively

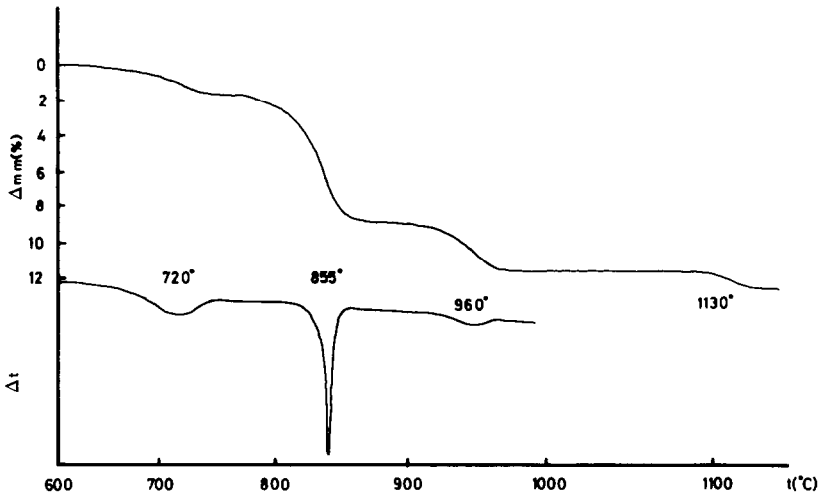

FIG. 3. DTA and TGA diagrams of $Ca_2Pt_3O_8$.

TABLE III

X-RAY DIFFRACTION PATTERN OF $Ca_2Pt_3O_8$ TAKEN WITH A GUINIER FOCUSING CAMERA[a]

a = 6.196(1) Å
c = 15.404(3) Å

d_{cal}	d_{obs}	$h\ k\ l$
5.13	5.13	0 0 3
5.07	5.07	1 0 1
4.40	4.40	0 1 2
3.129	3.129	1 0 4
2.643	2.642	0 2 1
2.567	2.565	0 0 6
2.533	2.545	2 0 2
2.201	2.200	0 2 4
2.023	2.023	2 0 5
1.7944	1.7940	2 1 4
1.7014	1.7026	0 2 7
1.6940	1.6934	1 2 5
1.6890	1.6895	0 3 3
1.5643	1.5643	2 0 8
1.5489	1.5492	2 2 0
1.4829	1.4828	2 2 3
1.4611	1.4647	3 1 2

[a] Fe$K\alpha_1$ wavelength.

in air and in tetrachloromethane (d = 1.5867); a pellet was obtained by cold pressing.

2.6. Powder X-ray diffraction. The cell parameter measurements and phase identification were accomplished with a Guinier focusing camera with Fe$K\alpha_1$ radiation (λ = 1.93597 Å) and using an internal standard of Si (99.99%). Intensity data were collected, using a Siemens Kristalloflex D500 diffractometer (λ = 1.93728 Å), at 0.02° 2θ intervals and 6 sec/step. The integrated intensities were obtained by adding the step counts under each peak and then subtracting the average background between the beginning and the end of each peak.

2.7. Neutron diffraction. Neutron diffraction patterns at room temperature were collected using the diffractometer D1B at the Institut Laue-Langevin, Grenoble. A wavelength of 2.5186 Å was selected using a pyrolytic graphite monochromator, with high-order contamination suppressed by a set of pyrolytic graphite filters. The sample was inserted in a standard vanadium can (ϕ10 × 50 mm). The diffractometer has a 400-cell multidetector covering 80° 2θ. The data were collected in two steps (low and high angles) of about 4 hr each, between 24 and 142° 2θ.

Integrated intensities were obtained by fitting the shape of the Bragg peaks to Gaussians and the background to a first- or second-order polynomial (*9*).

2.8. Refinement calculations. The program MXD (*10*) was used for least-squares refinement of the structure. This program uses both X-ray and neutron data as input information and minimizes the function

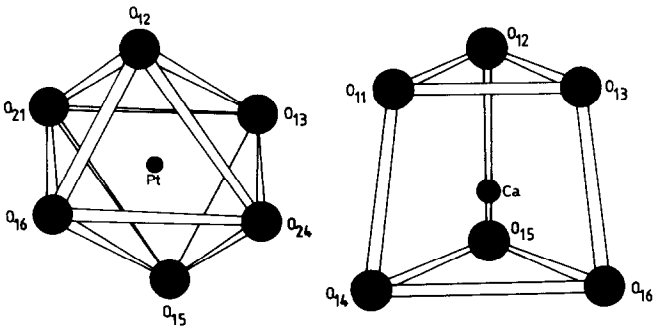

FIG. 4. Pt and Ca environments along the z axis.

TABLE IV

X-RAY DIFFRACTION INTENSITIES, L-P CORRECTED, OF $Ca_2Pt_3O_8$[a]

h k l	I_{cal}	I_{obs}	Weight[b]	h k l	I_{cal}	I_{obs}	Weight[b]
0 0 3				0 0 12	79.67	74.28	1.16
1 0 1	143.04	151.13	0.813	4 0 4	118.60	88.94	1.06
0 1 2	69.34	56.97	1.32	2 0 11			
1 0 4				3 0 9			
1 1 0	90.43	86.62	1.07	1 3 7			
0 1 5				0 4 5			
1 1 3				2 1 10			
0 2 1	489.13	453.04	0.470	3 2 1			
0 0 6	94.20	120.05	0.913	2 3 2	624.39	648.52	0.393
2 0 2	375.85	337.08	0.545	3 1 8			
0 2 4	155.22	142.94	0.836	1 1 12			
1 0 7				3 2 4			
2 0 5				1 4 0	143.12	124.34	0.897
2 1 1	475.96	461.21	0.466	1 0 13			
1 1 6				1 2 11			
1 2 2	96.63	114.63	0.935	2 2 9			
0 1 8				4 0 7			
2 1 4				2 3 5			
3 0 0	163.87	154.75	0.804	4 1 3	792.18	840.73	0.345
0 0 9				0 4 8	208.37	221.61	0.672
0 2 7				0 2 13			
1 2 5				0 1 14			
3 0 3	652.60	718.69	0.373	3 2 7	230.12	299.34	0.578
2 0 8	315.26	324.42	0.555	3 0 12			
2 2 0	435.58	425.30	0.485	2 3 8			
1 1 9				0 5 4			
2 1 7				3 3 0			
2 2 3				0 0 15			
1 0 10				2 1 13			
1 3 1				3 1 11			
3 0 6				2 0 14			
3 1 2	693.90	736.59	0.368	5 0 5			
1 2 8				3 3 3			
1 3 4	131.66	116.61	0.926	4 0 10			
0 1 11				2 4 1			
3 1 5				4 2 2	1256.65	1142.33	0.296
0 2 10							
4 0 1							
2 2 6							
0 4 2	1142.16	1202.84	0.288				

[a] Comparison between observed and calculated values.

[b] $w \propto I_0^{-1/2}$.

$\Sigma w^2(F_0^2 - F_c^2)^2$, where the weight, w, for each reflection is set equal to $1/\sigma_{F^2}^2$ for neutron data, and to $I_{obs}^{-1/2}$ for X-ray diffraction data. Scattering factors for neutral atoms and for real and imaginary anomalous dispersion coefficients for Fe$K\alpha$ radiation were taken from (*11*). The neutron scattering lengths were taken from (*12*).

TABLE V

NEUTRON DIFFRACTION INTENSITIES, LORENTZ FACTOR CORRECTED, OF $Ca_2Pt_3O_8$[a]

h k l	I_{cal}	I_{obs}	Weight[b]	h k l	I_{cal}	I_{obs}	Weight[b]
0 0 3				0 1 8			
1 0 1	171.48	174.00	2.50	2 1 4			
0 1 2	142.10	141.00	2.00	3 0 0	595.44	589.00	0.256
1 0 4				0 0 9			
1 1 0	108.59	105.00	2.50	0 2 7			
0 1 5				1 2 5			
1 1 3				3 0 3	1987.87	1981.00	0.196
0 2 1	310.29	285.00	0.588	2 0 8			
0 0 6				2 2 0	3662.26	3969.00	0.057
2 0 2	748.86	792.00	0.588	1 1 9			
0 2 4	100.71	31.26	0.303	2 1 7			
1 0 7				2 2 3			
2 0 5				1 0 10			
2 1 1	2305.76	2233.00	0.250	1 3 1			
				3 0 6			
				3 1 2	1728.45	1987.00	0.015

[a] Comparison between observed and calculated values.
[b] $w \propto 1/\sigma_{F^2}^2$.

3. Results and Discussion

3.1. Preparation and Identification

The X-ray diffraction patterns of $CaPt(OH)_6$ are in agreement with the data of Trommel and Lupprich (*13, 14*). The yellow $Ca_2Pt_3O_8$ powder is not very crystalline (the $K\alpha_1$ and $K\alpha_2$ reflections of the diffractometer patterns overlap even at high angles). Changing the conditions of hydrothermal synthesis—increasing the temperature and/or time of treatment, as well as the cooling rate—did not appreciably affect the crystallinity of the product. Pt impurities were always detected in the X-ray diffraction patterns. The shape of the larger crystals obtained in one of the experiments is shown in Fig. 1. They are hexagonal platelets.

The product is insoluble in water, nitric acid, hydrochloric acid, or hot aqua regia, but it is soluble in hot hydrobromic acid. Therefore, the product could be purified of Pt contamination with hot aqua regia. Infrared spectra (Fig. 2) of the resulting product showed none of the characteristic absorption bands for O–H bonds and H_2O at 1600, 2300, and 3200 cm^{-1}.

3.2. Thermal Stability

To follow the process of decomposition, the product was heated in a furnace at different temperatures and after each treatment, an X-ray diffraction pattern was obtained. The results are summarized in Table I.

TABLE VI

FINAL REFINED ATOMIC POSITIONS AND ISOTROPIC TEMPERATURE FACTORS[a]

Atom	Site	Coordinates			Thermal parameters (Å²)
Pt	9*d*	0.5	0	0	0.2 (1)
Ca	6*c*	0	0	0.145 (3)	0.4 (1)
O(1)	18*h*	0.482 (2)	−0.482 (2)	0.404 (1)	0.5 (fixed)
O(2)	6*c*	0	0	0.397 (4)	0.5 (1)

[a] Error standard deviations are given in parentheses and refer to the last digit. $Ca_2Pt_3O_8$; space group $R\bar{3}m$ (No. 166); $z = 3$.

TABLE VII

SIGNIFICANT INTERATOMIC DISTANCES (IN Å) IN THE $Ca_2Pt_3O_8$ STRUCTURE

Ca–Ca = 3.64 (3)
Pt–Pt = 3.10 (1)

Ca^{2+} environment[a]		Pt^{4+} environment[a]	
O_{11}–O_{12}[b] = 2.77 (1)	Ca–O_{11} = 2.42 (3)	O_{21}–O_{15} = 3.11 (4)	O_{13}–O_{15} = 2.77 (1)
O_{14}–O_{15} = 3.43 (1)	Ca–O_{14} = 2.29 (3)	O_{12}–O_{13} = 2.93 (1)	O_{13}–O_{24} = 2.61 (4)
O_{11}–O_{14} = 2.99 (1)		Pt –O_{21} = 2.04 (4)	Pt –O_{12} = 2.02 (1)

[a] See Fig. 6.
[b] Oxygen notation: O_{ij}, where i refers to the numbering O(i) given in Table VI.

TGA and DTA were also performed (see Fig. 3). The TGA curve shows four weight losses and the DTA curve shows the endothermic peaks corresponding to the first three steps. The weight losses resulting from the decomposition reactions are summarized in Table II. This table also includes the temperatures of decomposition found in the TGA diagram. The experimental weight loss for total decomposition (12.54%) agrees with the theoretical value of 12.10%.

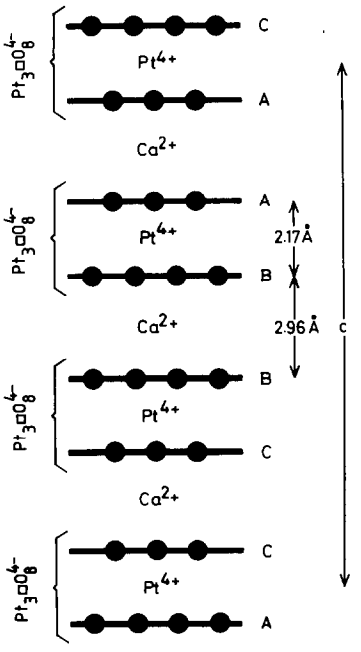

FIG. 5. Schematic representation of $Ca_2Pt_3O_8$ structure along the z axis.

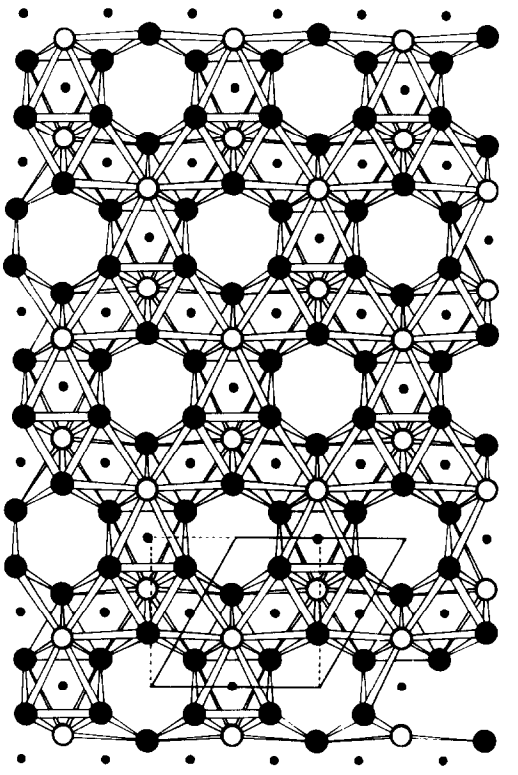

FIG. 6. Projection of the $Pt_3\square O_8^{4-}$ layer along the z axis. Small solid circles denote the Pt ions, large solid circles denote O(1), and open circles denote O(2). The hexagonal and orthorhombic cells are also sketched.

3.3. Structure Determination

The diffraction data obtained with a Guinier focusing camera are given in Table III. The reflections are indexed with a hexagonal cell. All reflections verify the condition $-h + k + l = 3n$, no other extinction rule being observed. Possible space groups are $R3m$, $R\bar{3}m$, $R32$, $R3$, and $R\bar{3}$. The experimental density measured on a pressed pellet is 6.6 and the calculated density assuming three formula units per hexagonal cell is 7.41.

The refinement was performed in space group $R\bar{3}m$. Previous trials in space groups of lower symmetry gave less accurate results. Assuming 9 Pt atoms in the unit cell, only a limited number of distributions among the sites of $R\bar{3}m$ is possible. Trial and error methods using only X-ray data allow Pt to be located in the position 9*d*. Further calculations and geometrical considerations led to the positioning of calcium and oxygen at sites 6*c* and 18*h*, respectively. Treatment of neutron diffraction data allowed location of the remaining oxygen atoms at site 6*c*. After several cycles, the weighted reliability factor, R_w fell to 0.0408 for the neutron diffraction intensities and for the X-ray data R_w fell to 0.0866, giving a general R_w value of 0.0682. The isotropic temperature factors were also included in the refinements; however, the oxygen O(1) thermal parameter reached negative values, presumably because of an error in background estimation. Therefore the oxygen O(1) temperature factor in the final refinements was held fixed at an arbitrary value of 0.5 Å^2. In Tables IV and V the observed intensities are compared with final calculated values for both X-ray and neutron data. The final atomic positions are summarized in Table VI.

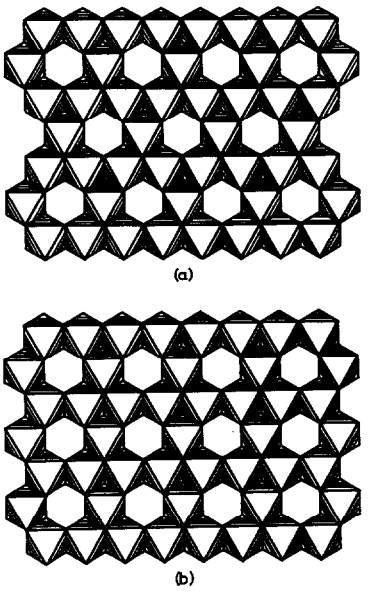

FIG. 8. $M_3O_8^{4-}$ octahedral layers in oxides $A_2M_3O_8$. (a) Hexagonal, Kagome layer. (b) Orthorhombic.

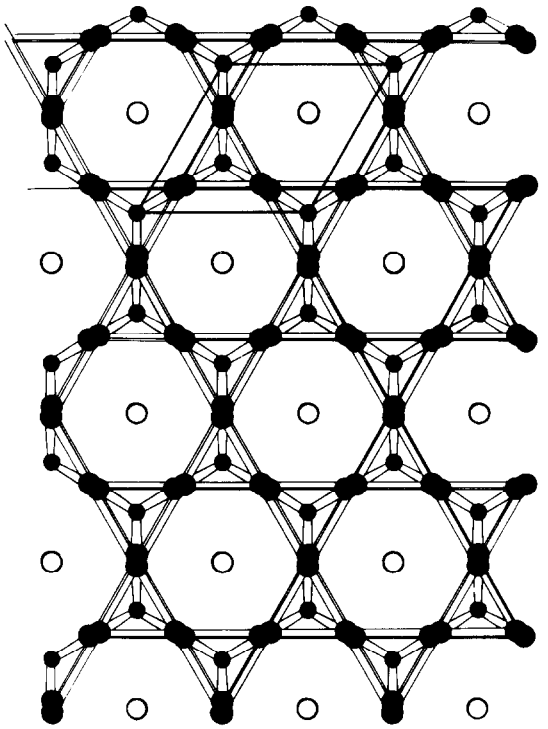

FIG. 7. Projection along the *z* axis of a Ca layer and the neighboring oxygen planes. Small solid circles denote Ca ions. Oxygen notation is as in Fig. 6. The hexagonal cell is also sketched.

3.4. *Description of the Structure*

The bond distances are summarized in Table VII and the coordination polyhedra of Pt and Ca are presented in Fig. 4. Pt is octahedrally coordinated with an average Pt–O distance of 2.02 Å; the value calculated from the ionic radii of Shannon (*15*) is 2.005 Å. The calcium environment is a slightly distorted trigonal prism with two sets of Ca–O distances; the average Ca–O distance is 2.36 Å and the calculated distance is 2.38 Å. The calcium bond strength calculated from the experimental data with the bond valence parameters given in Ref. (*16*) is 1.92, reasonably close to the expected value of 2. Every O(1) is bonded to two Pt^{4+} and one Ca^{2+} while O(2) is bonded only to three platinum atoms.

The most prominent feature of the $Ca_2Pt_3O_8$ structure is the alternate sequence of Pt and Ca layers along the *c* axis. The oxygen layers form compact layers packed along the *c* axis as follows, . . . *AABBC CAABBCC*. . . (see Fig. 5); Pt^{4+} ions occupy 75% of the octahedral holes between alternate pairs of oxygen close packed layers (see Fig. 6). From this point of view the $Pt_3\square O_8^{4-}$ sheets can be described as defective CdI_2 layers. This is to be related to the structure proposed for α-PtO_2 which is believed to have CdI_2 structure. In this respect it is worthwhile to mention that the *a* parameter of α-PtO_2 (*17*) is exactly half the *a* parameter of $Ca_2Pt_3O_8$.

$Pt_3\square O_8^{4-}$ layers found in $Ca_2Pt_3O_8$ are not loosely bonded as in α-PtO_2 but they are connected to each other by the calcium layer (Fig. 5). Ca^{2+} ions occupy 25% of prismatic holes between oxygen layers above and below the empty sites of the platinum layer; therefore the structure could be described alternatively as a framework of CaO_6 trigonal prisms which share side edges to build infinite two-dimensional layers in the *ab* plane (see Fig. 7).

The structure of $Ca_2Pt_3O_8$ with alternating (Ca^{2+}) and $(Pt_3O_8)^{4-}$ layers is reminiscent of the structure of $A_2^{2+}Mo_3O_8$ and $A_2^{2+}Mn_3O_8$ oxides. Indeed, the last two structures can also be described as an alternate stacking of $(A^{2+})_2$ and $(\square M_3O_8)$ defective layers. They differ essentially by the ordering of the vacant sites within the $\square M_3O_8$ layer: in the case of the molybdates, the vacancies are hexagonally ordered,

TABLE VIII

COMPARISON OF CELL OF CATION COORDINATION AND PARAMETERS AMONG $A_2M_3O_8$ OXIDES

Compound	Layer	A^{2+} coordination[a]	a'(Å)[b]	c'(Å)[b]	Space group	Reference
$Ca_2Pt_3O_8$	Kagome	TP	6.196	3 × 5.135	$R\bar{3}m$	This work
Nolanita	Kagome	T/O	5.854	2 × 4.648	$P6_3mc$	(*18*)
$Zn_2Mo_3O_8$	Kagome	T/O	5.759	2 × 4.952	$P6_3mc$	(*19*)
$Fe_2Mo_3O_8$	Kagome	T/O	5.777	2 × 5.029	$P6_3mc$	(*20*)
$Co_2Mo_3O_8$	Kagome	T/O	5.767	2 × 4.958	$P6_3mc$	(*20*)
$Mn_2Mo_3O_8$	Kagome	T/O	5.799	2 × 5.134	$P6_3mc$	(*20*)
$Co_2Mn_3O_8$	Mn_3O_8	T/O	5.743	2 × 4.681	$Pmn2_1$	(*21*)
$Zn_2Mn_3O_8$	Mn_3O_8	T/O	5.766	2 × 4.695	$Pmn2_1$	(*22*)
$Cd_2Mn_3O_8$	Mn_3O_8	TP	5.808	2 × 5.092	$C2/m$	(*23*)
$Mn_2Mn_3O_8$	Mn_3O_8	TP	5.724	2 × 4.879	$C2/m$	(*23*)
$Ca_2Mn_3O_8$	Mn_3O_8	TP	5.848	2 × 5.184	$C2/m$	(*24*)
$Cu_2Mn_3O_8$	Mn_3O_8	SP	5.635	2 × 4.717	$C2/m$	(*25*)

[a] TP, trigonal prismatic; T/O, tetrahedral and octahedral; SP, distorted square pyramidal.
[b] a', interplane spacing; c', interlayer spacing.

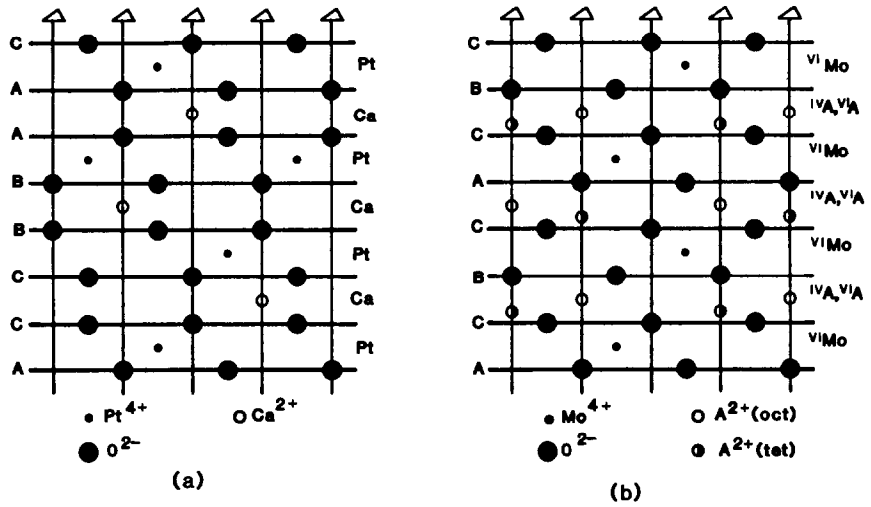

FIG. 9. Schematic representation along the z axis of (a) $Ca_2Pt_3O_8$ and (b) $A_2M_3O_8$.

thus giving rise to a Kagome layer (see Fig. 8a) whereas they form a rectangular one in the Mn_3O_8 layers (Fig. 8b). The stacking of the M_3O_8 layers depends on the size and bonding requirements of the intercalated cation A^{2+}. In the case of the molybdates (A^{2+} = Zn, Fe, Co, Mn) and isostructural nolanite, the A^{2+} cations are found in two positions with tetrahedral and octahedral coordination, respectively (Fig. 9b); the $A_2Mn_3O_8$ compounds are more complex and three different arrangements have been observed (Table VIII):

—tetrahedral and octahedral coordination as in the nolanite and molybdates: A^{2+} = Co, Zn

—trigonal prismatic coordination: A^{2+} = Cd, Ca, Mn

—distorted square pyramidal environment: A^{2+} = Cu.

$Ca_2Pt_3O_8$ with its Kagome layers (Fig. 6) and the trigonal prismatic coordination of the calcium (Fig. 9a) can thus be considered as intermediate between the nolanite and $Mn_2Mn_3O_8$ structures (Table VIII) and is the first example of a new $A_2M_3O_8$ type compound.

4. Conclusions

$Ca_2Pt_3O_8$ is a new ternary oxide whose structure can be described as being built up from defective CdI_2-like layers with composition $Pt_3\square O_8^{4-}$, with these layers held together by Ca^{2+} to form a three-dimensional framework. It is closely related to α-PtO_2 and to the two structural types nolanite and $Mn_2Mn_3O_8$.

Acknowledgments

The authors acknowledge Dr. Wolfers for computing advice and Dr. Bochu for SEM work; thanks are also due to Dr. P. Lacorre for helpful discussions. One of the authors (X.T.) would like to thank the Basque Government for financial support.

References

1. K. B. SCHWARTZ AND C. T. PREWITT, *J. Phys. Chem. Solids* **45**, 1 (1984).
2. B. GORDON, Powder Data File, Card No. 15-520, JCPDS, Swarthmore, PA.
3. I. S. SHAPLYGIN AND V. B. LAZAREV, *Mater. Res. Bull.* **10**, 903 (1975).
4. R. CZAYA, Powder Data File, Card No. 23-860, JCPDS, Swarthmore, PA.

5. C. L. McDaniel, Powder Data File, Card No. 23-862, JCPDS, Swarthmore, PA.
6. H. Ohsato, T. Sugimura, and K. Kugeyama, *J. Cryst. Growth* **51,** 1 (1981).
7. C. Laviron, Thèse, Grenoble, (1981).
8. C. T. Prewitt, K. B. Schwartz, and R. D. Shannon, *Acta Crystallogr. Sect. C* **39,** 519 (1983).
9. P. Wolfers, Programs for treatment of powder profiles, ILL, (1975).
10. P. Wolfers, To be published in *Appl. Cryst.*
11. "International Tables for X-ray Crystallography," Vol. III, Kynoch Press, Birmingham, (1974).
12. L. Koester and H. Rauch, Summary of Neutron Scattering Lengths, IAEA Contract 2517/RB, (1981).
13. M. Troemmel and E. Lupprich, *Z. Anorg. Allg. Chem.* **414,** 169 (1975).
14. M. Troemmel and E. Lupprich, *Naturwissen Schaften* **60,** 351 (1973).
15. R. D. Shannon, *Acta Crystallogr. Sect. A* **32,** 751 (1976).
16. I. D. Brown and K. K. Wu, *Acta Crystallogr. Sect. B* **32,** 1957 (1976).
17. H. R. Hoekstra, S. Siegel, and F. X. Gallagher, *Adv. Chem. Ser.* **98,** 39 (1981).
18. A. W. Hanson, *Acta Crystallogr.* **11,** 703 (1958).
19. G. B. Ansell, *Acta Crystallogr.* **21,** 482 (1966).
20. D. Bertrand and H. Kerner-Czeskleba, *J. Phys.* **36,** 379 (1975).
21. A. Riou and A. Lecerf, *Acta Crystallogr. Sect. B* **31,** 2487 (1975).
22. A. Lecerf, *C.R. Acad. Sci. Paris* **279,** 879 (1974).
23. H. R. Oswald and M. J. Wampetich, *Helv. Chim. Acta* **50,** 2023 (1967).
24. G. B. Ansell, *Acta Crystallogr. Sect. A* **34,** S157 (1978).
25. A. Riou and A. Lecerf, *Acta Crystallogr. Sect. B* **33,** 1896 (1977).